Adsorption of C2–C5 alcohols on ice: A grand canonical Monte Carlo simulation study

Julien Joliat, Sylvain Picaud, Antoine Patt, Pal Jedlovszky

Adsorption of C2-C5 alcohols on ice. A grand canonical Monte Carlo simulation study

Julien Joliat,[1] Sylvain Picaud,[1, a)] Antoine Patt,[1, 2] and P. Jedlovszky[3]
[1)] *Institut UTINAM UMR 6213, CNRS/Université de Bourgogne Franche-Comté, Besançon, France*
[2)] *Centro de Fisica de Materiales, CSIC - UPV/EHU, 20018 San Sebastian, Spain*
[3)] *Department of Chemistry, Eszterházy Károly University, Leányka u. 6, H-3300 Eger, Hungary*

(Dated: 16 May 2022)

In this paper, we report Grand Canonical Monte Carlo simulations performed to characterize the adsorption of four linear alcohol molecules, comprising between 2 and 5 carbon atoms (namely, ethanol, n-propanol, n-butanol, and n-pentanol) on crystalline ice in a temperature range typical of the Earth's troposphere. The adsorption details analysed at 228 K show that, at low coverage of the ice surface, the polar head of the adsorbed molecules tend to optimize its hydrogen bonding with the surrounding water, whereas the aliphatic chain lie more or less parallel to the ice surface. With increasing coverage, the lateral interactions between the adsorbed alcohol molecules lead to the reorientation of the aliphatic chains which tend to become perpendicular to the surface, the adsorbed molecules pointing thus their terminal methyl group up to the gas phase. When compared to the experimental data, the simulated and measured isotherms show a very good agreement, although a small temperature shift between simulations and experiments could be inferred from simulations at various temperatures. In addition, this agreement appears to be better for ethanol and n-propanol than for n-butanol and n-pentanol, especially at the highest pressures investigated, pointing to a possible slight underestimation of the lateral interactions between the largest alcohol molecules by the interaction potential model used. Nevertheless, the global accuracy of the approach used, as tested in tropospheric conditions, opens the way for its use in modeling studies also relevant to another (e.g., astrophysical) context.

I. INTRODUCTION

To date, dozens of molecular species, comprising up to 70 atoms for the largest ones, have been detected or strongly suspected to be present in the interstellar and circumstellar media by astronomical observations.[1] Some of them have also been detected in cold, solid environments, including water ice, although specific requirements for the corresponding observations often prevented definite conclusions to be drawn on their exact molecular compositions.[2] Water ice is indeed ubiquitous in the Universe,[3] covering, for instance, interstellar and cometary dust grains, where it is subject to, e.g., cosmic rays, UV irradiation and thermal reactions.[4,5] It is thus long supposed that water ice may significantly contribute to the formation of large molecules via a rich solid-state chemistry,[6,7] especially since it has been proven in laboratory experiments that, under astrophysical conditions, water ice may be an efficient catalyst or chemical reactant.[4,5] Then, easy release or, on the contrary, long trapping of these molecules by ice mantles on interstellar grains may impact on their detection in astrophysical environments. On the other hand, ice is also abundant in the Solar System, not only on Earth, but also in comets and in various planetary environments, such as Jovian satellites and Saturn's moons.[8] In the corresponding thermodynamic conditions, ice may be found in crystalline or amorphous phases, or even as clathrate hydrates.[2,3,9] There, these various forms of ice may also promote reactive heterogeneous chemistry or influence the partitioning of molecular species between ice and the surrounding fluid phase.[10–12]

Ice is also abundantly present in the Earth's atmosphere as snow flakes, hailstones as well as micrometer–sized particles in high altitude cirrus clouds. It is also found on the ground, in snowpacks or as sea ice. In these various conditions, ice surface temperatures may range from close to zero to as low as −80° C, opening thus the door to different physico-chemical processes. Thus, it is now well-recognized that ozone depletion in the stratosphere is promoted by specific chemical reactions that involve halogenated species initially trapped at the surface of ice nanoparticles in polar stratospheric clouds.[13]. Beside heterogeneous chemistry, incorporation into the bulk of ice or reversible trapping at its surface of ionic and molecular species may also have a direct impact on the lifetime of atmospheric trace gases via precipitation scavenging, differential release and vertical redistribution.[14–18]. Similarly, it has been recently inferred that selective trapping on ice may have influenced the measurements by *Cassini* of the gas phase abundances of some organic compounds in the geysers that are erupting from Enceladus' surface.[12]

The common feature of all these processes is that they

[a)] Electronic mail: sylvain.picaud@univ-fcomte.fr

strongly depend on the details of the interaction between the considered species and the surface of ice, especially the strength of the binding energy.[19] Thus, for years, numerous experimental studies have been devoted to the characterization of the behavior of various species on ice, with a special focus on the trapping of volatile (VOC) and semi-volatile (SVOC) organic compounds under tropospheric conditions.[15] Indeed, these species of both biogenic and anthropic origins are abundant in the atmosphere, where their photolysis and their reactions with ozone or OH and NO_3 radicals contribute significantly to the production of HO_2 and RO_2, i.e., the radical chemistry that may change the fate of the majority of other trace gases.[20] It thus appeared of primary importance to quantify in which proportion ice crystals can modify the atmospheric concentrations of the VOC and SVOC molecules that are suspected to strongly partition to ice because they most often contain oxygenated functional groups that may attach to the ice surface by forming hydrogen bonds.

Concomitantly, some of these experimental studies have been nicely complemented by theoretical investigations based either on quantum chemistry approaches[19] or on numerical simulations using classical force fields.[21] Indeed, these approaches can give information at the molecular scale on the adsorption process, which may then be compared with or added to the available experimental data. Modeling studies can also be performed to characterize the considered systems under specific conditions that are not easily accessible to the experiments. Among the various simulation approaches that can be used, the grand canonical Monte Carlo (GCMC) method[22,23] has proven to be particularly suitable to model the interaction between VOCs/SVOCs and ice[24–43] since its first application was devoted to the adsorption of methanol on ice under tropospheric conditions.[24] In particular, the GCMC method can be used to simulate the adsorption isotherms by calculating the number of molecules that are adsorbed at the surface of ice as a function of the chemical potential or, equivalently, the partial pressure of the gas species under consideration.[21] In addition, thorough statistical analyses of the data issued from the GCMC simulations can give access to, *e.g.*, the adsorption energy, the monolayer saturation coverage and the molecular orientations at the ice surface. Moreover, the simulation of the adsorption isotherms up to the pressure of the saturated vapor can also be used to check if the adsorption follows the Langmuir model, an assumption that is usually made on the basis of experimental data, although experiments are most often limited to submonolayer coverages.[26,27]

However, it is worth noting that the results of any simulation strongly depend on the models and on the corresponding parameters that have been used to calculate the interaction energies. As a consequence, validating the accuracy of these parameters is a required step before any definite conclusion can be drawn from the results of the calculations. This can tentatively be done by comparing, when possible, the simulated isotherms to those obtained experimentally under similar conditions.[24,27] Thus, in a previous study, we chose the methanol molecule for such a comparison, because we could get high-quality, reproducible experimental data on this system and, concomitantly, a well-tested simple potential model for the methanol-water interactions was available to be used in the simulations.[24] Overall, a fair agreement was found between simulated and experimental data, although a slight (about 5 K) temperature shift in the simulation data was evidenced, because the isotherm calculated at 200 K fell between the experimental isotherms obtained at 203 and 208 K. This shift was attributed to a slight underestimation of the strength of the interaction between water and methanol with respect to that of the methanol-methanol interaction. It is worth mentioning that the interaction potential model used in this study was specifically developed to describe the methanol-water interaction and, thus, it cannot be used to study larger alcohol molecules. Such molecules, however, would also deserve specific attention due to their abundance in the Earth's atmosphere[44] and to their detection almost everywhere in Space.[45]

To properly investigate the behavior of these larger alcohol molecules at the ice surface, it is necessary to use suitable interaction models in the simulations, which combine relative simplicity and good transferability from one system to another. In this respect, the AUA4 force field, specially developed for alcohol and polyalcohol molecules, appears to be a good candidate,[46] provided that, in combination with a suitable water potential, it reproduces accurately enough at least some of the experimental results. In this goal, we benefit here from the fact that the adsorption behavior of different alcohols on crystalline ice has been thoroughly investigated experimentally in the temperature range between 213 and 245 K as a function of the molecular size.[47] Thus, by performing here GCMC calculations to simulate the adsorption isotherms of four linear alcohol molecules (from ethanol to n-pentanol) on ice, and comparing the corresponding results to the measured isotherms, we aim at testing the ability of the AUA4 potential model[46] of properly describing the adsorption of alcohol molecules on ice.

Then, by using experimental results obtained under conditions that are typical of the Earth's troposphere (and that are, as far as we know, the only available set of experimental data for this series of molecules), we hope to obtain at least a partial view on the accuracy vs. limitations of the AUA4 interaction model and of its possible transferability to conditions that would be rather relevant for other, *e.g.*, astrophysical, environments like the interstellar medium or the atmosphere of Enceladus.

The paper is organized as follows. Technical details of the simulations are given in section II. The corresponding results are presented and discussed in detail section III. Finally, the main conclusions of this work are summarized in section IV.

II. SIMULATION DETAILS

Here, the adsorption of ethanol (C_2H_6O), n-propanol (C_3H_8O), n-butanol ($C_4H_{10}O$), and n-pentanol ($C_5H_{12}O$) on I_h ice[48] is investigated by means of GCMC simulations performed at different temperatures, ranging from 213 K to 245 K, according to the temperature range considered experimentally.[47]

The rigid TIP4P/ice model is used to represent the water molecules, because it has been specifically designed to cope with solid-phase properties of water.[49] With this model, the predicted melting temperature of hexagonal ice (Ih) at 1 bar is around 270 K,[50] *i.e.*, well above the temperatures considered in the present study.

The four alcohol molecules considered here are represented by the flexible AUA4 force field.[46] This model has been chosen because it was specifically developed to model liquid properties of a large series of alcohols with transferability to primary alcohols (methanol, ethanol, propan-1-ol, hexan-1-ol, octan-1-ol), secondary alcohols (propan-2-ol), tertiary alcohols (2-methylpropan-2-ol), phenol, and diols (1,2-ethanediol, 1,3-propanediol, 1,5-pentanediol).[46] Moreover, this potential model has been shown to give convincing results when used to characterize the adsorption of propanol on ice at 236 K under conditions typical of the environment of Enceladus.[43]

Both TIP4P/ice and AUA4 models are parametrized as sums of pairwise dispersion-repulsion and electrostatic terms, defined by Lennard-Jones (LJ) and Coulomb interactions, respectively. Interactions between water and alcohol molecules are thus calculated in a similar way, using the usual Lorentz-Berthelot combination rules for the determination of the cross LJ parameters[23].

The LJ contributions to the interaction potential are truncated at a cutoff distance equal to half the smallest edge length of the simulation box, and long-range corrections have been taken into account.[51] The electrostatic interaction is calculated by using the method of Ewald summation.[23]

A. GCMC simulations

The GCMC simulations are performed in a simulation box of dimensions $L_x = 35.926$ Å $\times$ $L_y = 38.891$ Å $\times$ $L_z = 100$ Å, in which an ice crystal has been previously introduced, which contains 2880 water molecules, arranged in 18 layers, along the (0001) crystallographic direction (*i.e.*, the z axis). Note that the values of L_x and L_y have been chosen according to the periodicity of the ice crystal along the x and y axes. By contrast, a large empty space has been created above and below the ice crystal, along the z axis, leading to the existence of two gas/ice interfaces in the simulation box. Periodic boundary conditions are applied along all the three axes of the simulation box, x, y and z. The same simulation box has been used for all the temperatures considered here, because variations of the ice lattice parameters have been measured to be negligible in this temperature range.[52]

All the simulations are performed using the Monte Carlo general purpose GIBBS software package.[53] For the GCMC simulations, carried out in the grand canonical ensemble, a typical run starts with an equilibration phase of 2–9$\times10^8$ Monte Carlo (MC) steps, depending on the fugacity, followed by a production stage ranging from 1 to 2×10^8 MC steps. In these simulations, alcohol molecules are considered to be flexible, and five types of Monte Carlo moves are used, namely insertion, deletion, translation, rotation and configurational-biased regrowth (i.e., change of the internal molecular configuration), each of which is performed with the same probability of 20%. Note that for efficient insertion and partial regrowth moves, the Gibbs code uses the configurational-bias Monte Carlo technique associated with a reservoir of thermodynamically relevant trial internal molecular conformations generated beforehand.[51,53] By contrast, the water molecules of the ice substrate are kept rigid and, thus, they are only subject to rotation and translation moves, performed with equal trial probabilities.

It is noteworthy that, instead of the chemical potential, the GIBBS code allows to work directly with the fugacity, which is the most convenient way to simulate adsorption isotherms directly comparable to experimental data, as far as a reliable conversion from fugacity to pressure can be achieved.[53] The relation between fugacity and pressure could be obtained via a classical thermodynamic model, such as an equation of state, or through activity coefficients when available. However, this may not be consistent with the potential model used in the simulations to calculate the intermolecular interactions. Instead, it is possible to use a Widom procedure that relies on test insertions during a preliminary NPT simulation of the fluid phase at the desired pressure.[51,53] This procedure, briefly recalled below, is based on the determination of the excess chemical potential of inserted species and, thus, it takes into account, in an adequate fashion, the force field used in the simulations and the possible non ideality of the adsorbed species.[54]

B. Widom insertion tests

In the Widom procedure, a series of Monte Carlo simulations in the (N, p, T) ensemble are first performed for each species under consideration, using a large cubic simulation box of the size of 3.10^4 Å $\times$ 3.10^4 Å $\times$ 3.10^4 Å, consisting of 300 alcohol molecules. In these simulations, the molecules have been subject not only to translational and rotational MC moves, but also to internal configuration changes, with trial probabilities of 30% for translation, 30% for rotation, 35% for configurational-bias regrowth, and 5% for volume change of the whole system.

Once the system has reached thermodynamic equilibrium (*i.e.*, after an equilibration period of 5×10^7 MC steps, when energy, volume and density do not fluctuate more than a few tenth of percent around their average

values), the chemical potential of the alcohol species is calculated as follows.[55] During 10^8 additional MC steps, a test alcohol molecule is randomly inserted into the system and the excess potential energy ΔU_{N+1} due to its addition is calculated. In fact, this operation is similar to the insertion move in the grand canonical ensemble, but without actually accepting or rejecting the insertion of the molecule. The trial probabilities of the MC moves during this phase are set to 20% for translation, 20% for rotation, 9% for configurational-bias regrowth, 1% for volume change, and 50% for test insertion.

The excess chemical potential, μ^{ex}, of the alcohol species, is calculated then by averaging over 10^6 MC steps the energetic contributions of the test molecules according to the following equation[51,55]

$$\mu^{ex} = \mu - \mu^0 = -k_B T \ln \left\langle V \exp\left(-\frac{\Delta U_{N+1}}{k_B T}\right)\right\rangle_{\{N,p,T\}} \quad (1)$$

with μ^0 being the reference chemical potential and V the fluctuating volume of the simulation box.

The obtained values of μ^{ex} are then easily converted to fugacity through usual thermodynamic equations[51], giving thus the correspondence between the fugacity and the desired pressure. This allows the determination of the fugacity coefficient, defined as

$$\varphi = \frac{f}{P} \quad (2)$$

which is an indication of the non-ideality of the system under consideration.

III. SIMULATION RESULTS AND DISCUSSIONS

A. Adsorption isotherms of ethanol, n-propanol, n-butanol and n-pentanol on ice at 228K

Let us first present the results of the GCMC simulations for ethanol, n-propanol, n-butanol, and n-pentanol molecules, adsorbed on ice I_h at 228 K, a temperature at which experimental results are available for these four species.[47]

The average number $\langle N\rangle$ of alcohol molecules found in the basic simulation box is shown in Fig. 1 as a function of the alcohol fugacity for each species under consideration. Note that because the alcohol molecules are almost never found isolated in the vapor phase above the ice surface, or dissolved in the bulk ice phase, the $\langle N\rangle$ vs. fugacity curves actually correspond to adsorption isotherms on ice.

Overall, the four simulated isotherms exhibit similar shape. At low fugacity values, a rapid increase of the number of adsorbed molecules $\langle N\rangle$ is observed, which corresponds to the building up of the adsorption layer. Then, in a broad range of values, the change of the fugacity results only in a small variation of $\langle N\rangle$, which is a strong indication of the formation of a stable monolayer of alcohol molecules at the ice surface. Finally, at higher fugacity values, the isotherm exhibits a sudden jump at the threshold value f_0 of the fugacity, which can be attributed to the 3-dimensional condensation of the alcohol molecules. As consequence, no more simulations are performed in this high fugacity range above f_0.

It is interesting to mention that the f_0 value decreases when the size of the alcohol molecule increases, in accordance with the values of the corresponding saturated vapor pressures, which are, however, available at higher temperatures.[56]

To study the alcohol adsorption isotherms in the context of the Langmuir theory, which is often used to interpret the experimental data,[15] the $\langle N\rangle$ vs. fugacity curves are converted to the more conventional Γ vs P/P_0 form, where

$$\Gamma = \frac{\langle N\rangle}{2L_x L_y} \quad (3)$$

is the surface concentration of the adsorbed molecules, the factor 2 in the denominator accounting for the presence of two gas/ice interfaces in the simulation box. Pressure values are calculated from fugacities using the Widom Monte Carlo procedure described above. Similarly, P_0 values (equal to about 45.0, 10.0, 2.0 and 0.3 Pa for ethanol, n-propanol, n-butanol and n-pentanol, respectively) have been deduced from the f_0 values directly measured on the simulated isotherms by using Eq. 2 with the corresponding values of φ equal to 1, 0.974, 0.876, and 0.766 for ethanol, n-propanol, n-butanol and n-pentanol, respectively. Note that the values that are significantly smaller than unity indicate the large non-ideality of the corresponding systems, as calculated with the AUA4 interaction potential used here.

Note that these P_0 values can, at least qualitatively, be compared to the corresponding pressures of the saturated vapor, as extrapolated down to 228 K from higher temperature measurements using the Antoine equation. Considering two different sets of Antoine coefficients avalaible in the literature[56,57], the experimental values of P_0 are estimated to lie in the following ranges : [30.07 – 45.07] Pa , [5.22 – 7.33] Pa, [0.25 – 0.32] Pa and [0.04 – 0.05] Pa, for ethanol, n-propanol, n-butanol and n-pentanol, respectively. Thus, from the comparison between the P_0 values issued from the simulations at 228 K (which strongly depend on the interaction potential model via the conversion from fugacity to pressure) and those extrapolated from experiments, it may be inferred that the interaction potential model used here performs probably better for ethanol and n-propanol than for n-butanol and n-pentanol to represent the intermolecular interactions between these alcohol molecules.

The Langmuir fits of the simulated isotherms are shown in Fig. 2 for the four alcohol molecules considered

here. They are based on the following equation :

$$\Gamma = \Gamma_{\max} \frac{P_{\rm rel} K}{P_{\rm rel} K + 1} \tag{4}$$

where $\Gamma_{\max}$ denotes the surface density at the saturation of one adsorption layer on ice, and K is the Langmuir partitioning coefficient. In this equation, the relative pressure is defined as $P_{\rm rel} = P/P_0$. As it can be seen on Fig. 2, the behavior of, *e.g.*, ethanol on ice at 228 K can be well represented by the Langmuir isotherm only up to the relative pressure of about 0.1, i.e., in a pressure range for which the lateral interactions between the adsorbed molecules are supposed to remain weak, and the molecules, bound to similar adsorption sites, are more or less isolated from each other. At higher relative pressure values, the simulated isotherm clearly departs from the Langmuir behavior. The situation is very similar for n-propanol, for which the Langmuir behavior seems also preserved up to $P_{\rm rel} \sim 0.1$, as previously observed at 236 K.[43] For the two other, larger, alcohol molecules, the Langmuir isotherm cannot be satisfactorily fitted even below $P_{\rm rel} \sim 0.05$. Thus, a detailed analysis of the adsorption layer is required to better characterize the trapping of the four alcohol molecules considered here on ice, and to explain the non-Langmuir behavior.

B. Properties of the adsorption layers

To investigate more precisely the adsorption behavior of the alcohol molecules considered here, four different values of the fugacity have been selected, illustrating four different typical situations on the ice surface (see Fig. 1). Thus, System 1 corresponds to a low fugacity value, where only very few isolated molecules are adsorbed at the surface, whereas System 2 is chosen to be at a fugacity value which likely corresponds to an unsaturated adsorption monolayer (increasing part of the isotherm, before the plateau starts in Fig. 1). For System 3, the fugacity value is chosen just below the point of condensation, while the condensed phase defines System 4. For each situation, configurations are saved every 2×10^4 steps during the production phase of the simulations, thus providing a set of $5–10 \times 10^3$ sample configurations (depending on the number of molecules adsorbed at the surface) for a detailed statistical analysis of the adsorbed phase.

1. Density profiles

The number density profiles calculated at 228 K along the z axis of the simulation box for the four C2-C5 alcohols considered here are shown in Fig. 3. In calculating these profiles, the position of an alcohol molecule has been represented by that of its center of mass and all the profiles shown are averaged over the two interfaces present in the basic box. In addition, the number density profile for the water molecules of the ice phase is also given on the same Figure, for reference. Notice that because these profiles $\rho_{\rm CM}(z)$ are calculated for the centers of mass of flexible molecules, the larger the molecule, the wider the peak of the distribution could be due to the various possible molecular configurations.

As shown in Fig. 3, the number density profile $\rho_{\rm CM}(z)$ calculated for System 1 exhibits only one very small peak, located near the ice surface, for all the four alcohol molecules considered here. This indicates that only very few molecules are trapped at the ice surface in this situation. A similar behavior is obtained for System 2, however with a larger intensity of the single peak observed in $\rho_{\rm CM}(z)$, which thus corresponds to a larger number of adsorbed alcohol molecules on ice, forming a single unsaturated monolayer at the surface. Upon approaching the point of condensation (corresponding to the fugacity value f_0), this monolayer becomes progressively more saturated, as evidenced by the gradual increase of the density peak located at a contact distance from the ice surface (System 3). Note that this peak also slightly shifts to larger z values, suggesting a reorientation of the molecular axes corresponding to a higher position of the centers of mass, this effect being thus especially more pronounced for the larger molecules. In addition, $\rho_{\rm CM}(z)$ for ethanol clearly exhibits additional broader peaks extending on the gas phase side, showing thus that traces of additional layers already occurs for System 3, *i.e.*, at fugacity values slightly below the condensation threshold. By contrast, the adsorption layer for the larger alcohol molecules remains mainly monomolecular (i.e., one single peak is obtained in $\rho_{\rm CM}(z)$ for System 3) up to the 3D condensation of the adsorbate. Finally, for the fugacity value corresponding to System 4, condensation has already occured for each alcohol considered here, as indicated by the large extension of $\rho_{\rm CM}(z)$ into the whole volume of the simulation box above the ice surface.

2. Energy profiles

To get insight into the energetic background of the adsorption process, the distributions of the energy between one adsorbed alcohol molecule and ice (U_{ads-w}), and between this alcohol molecule and the other adsorbed molecules ($U_{ads-ads}$) have been calculated at 228 K, and they are shown in Fig. 4. Note that these distributions are only given for Systems 1–3, i.e., before condensation has occurred.

As it can be seen, for System 1, *i.e.*, at very low surface coverage, the $P(U_{ads-w})$ distribution exhibits a single, rather broad, peak for each alcohol molecule considered here. Meanwhile, the corresponding $P(U_{ads-ads})$ distributions for ethanol and n-propanol (Fig. 4a and b) are also characterized by a single peak, located near zero, which indicates that, in this situation, these molecules are nearly isolated from each other on the ice surface.

Thus, for these two molecules, the values of the maximum of the distribution in U_{ads-w} for System 1, i.e., -69 and -67.0 kJ.mol^{-1}, for ethanol and n-propanol, respectively, can serve as estimates for the heat of adsorption at infinitely low coverage. Note that these values agree quite well with the corresponding experimental estimations of the enthalpy of adsorption (-61.9 ± 1.7 and -68.2 kJ.mol^{-1} for ethanol and n-propanol, respectively).[47]

The situation is a bit more complicated for the larger n-butanol and n-pentanol molecules, because at the low surface coverage characterizing System 1, the peak located near zero in the $P(U_{ads-ads})$ distributions is much wider than for the smaller alcohol molecules, and extends down to about -20 kJ.mol^{-1} (Fig. 4c and d). This clearly indicates that the adsorbed n-butanol and n-pentanol molecules cannot be considered as being isolated from each other on the ice surface even in System 1. Unfortunately, it would not be very relevant, from a statistical point of view, to investigate lower coverages, because they would correspond to a vanishingly small number of adsorbed alcohol molecules at the surface. These features thus prevent any rigorous determination of the heat of adsorption at infinitely low coverage from the present GCMC simulations of n-butanol and n-pentanol on ice, although the energy values corresponding to the maximum of the $P(U_{ads-w})$ distributions for these two molecules, *i.e.*, -71 kJ.mol^{-1}, can compare fairly well with the corresponding experimental estimations of the enthalpy of adsorption (-67.8 ± 3.8 and -71.5 ± 6.7 kJ.mol^{-1} for n-butanol and n-propanol, respectively).[47]

Considering the fact the the energy of a hydrogen bond is approximately -25 kJ.mol^{-1} for an ideal hydrogen-bonding geometry, and usually less in condensed phases, the above mentioned values indicate that the four alcohol molecules typically form three hydrogen bonds with the water molecules at low coverages of the ice surface.

When increasing the surface coverage up to the monolayer saturation (i.e., when considering System 3), the main peak in $P(U_{ads-w})$ shifts toward higher energy values (typically around -40 kJ.mol^{-1}), while the one in $P(U_{ads-ads})$ shifts toward lower values for all the four alcohol molecules considered here. This indicates a large increase of the lateral interactions at the expense of the interaction with ice. Note that this feature becomes even more pronounced with increasing size of the adsorbed molecule, the main peak in $P(U_{ads-ads})$ being located around -42, -47, -60 and -64 kJ.mol^{-1} for ethanol, n-propanol, n-butanol and n-pentanol, respectively. This could be related to adsorbed configurations in which the aliphatic chains are oriented perpendicular to the ice surface, as illustrated by the snapshots given in Fig. 3. Also, for System 3, the $P(U_{ads-w})$ distribution exhibits an additional peak around -10 kJ.mol^{-1}, especially in the case of ethanol, which can be related to the few molecules that are already adsorbed above the first layer being in contact with ice. Meanwhile, the $P(U_{ads-ads})$ distributions exhibit a large and a small peak, rather than a single one, as for System I. These two peaks could correspond to different numbers of hydrogen bonds formed between neighboring alcohol molecules.

3. Orientations

The characterization of the adsorption layer can be completed by the analysis of the molecular orientations at the surface of ice. Unfortunately, this is not a trivial task because the alcohol molecules are flexible in our simulations. Thus, these orientations cannot be unambiguously described by only two polar coordinates, as usually done when considering the orientation of rigid bodies relative to an external direction.[58] Rather, we use here three angles, defining the orientations of the molecular axis (θ_1), the CO vector, pointing from the alcoholic C to the O atom (θ_2), and the OH vector, pointing from the O to the H atom of the hydroxylic group (θ_3) with respect to the vector z normal to the gas/ice interface, pointing from the ice to the gas phase, as in our previous study.[43] Note that because the molecular axis is defined by the C–C vector pointing from the terminal aliphatic group (CH_3) to the alcoholic one, a value $\theta_1 = 0$ corresponds to a situation where the molecular axis is oriented perpendicular to the ice surface, the alcoholic group pointing up to the gas phase. Similarly, the values $\theta_2 = 0$ and $\theta_3 = 0$ correspond to configurations where the CO and OH vectors are oriented perpendicular to the ice surface.

The orientational distributions are given in Fig. 5 and Fig. 6, for the smaller (ethanol and n-propanol) and the larger (n-butanol and n-pentanol) alcohol molecules, respectively.

Overall, for the angle θ_1, these distributions exhibit similar behavior for the four alcohol molecules at the very low surface coverage corresponding to System 1, *i.e.*, a single, rather broad, peak is obtained with its maximum in the range of $\cos\theta_1$ values between -0.3 and -0.4, corresponding to θ_1 values between 107° and 113° . This can be related to tilted orientations of the C–C axis in the adsorption sites, *i.e.* a situation for which the OH group is closer to the ice surface than the methyl group. Note, however, that this single peak in the distribution $P(\cos\theta_1)$ has a rather large full width at half maximum (FWHM), equal to about 30°, that thus comprises, in fact, θ_1 values in the range of [90–135]°, corresponding to configurations of the molecular axes varying from the strictly parallel alignment to the ice surface to really tilted ones.

Upon increasing the coverage, System 2 presents the same characteristics as System 1, whereas for System 3, the four alcohol molecules reorient at the ice surface as shown by the shift of the main peak in the $P(\cos\theta_1)$ distributions, to values around -0.94. This reorientation thus tends to lift up the molecules ($\theta_1 \sim 160°$), keeping, however, their polar head pointing down to the ice surface. It also clearly appears that some other orientations

of the molecular axis are allowed, as indicated by the large extension of the distribution. For instance, a few adsorbed n-butanol and n-pentanol molecules may stay almost flat in System 3, as shown by small peak around $\cos\theta_1 = 0$ in Fig. 6.

When looking more precisely at the orientation of the polar head of these molecules, i.e., when considering the angles θ_2 and θ_3, Fig. 5 and Fig. 6 clearly exhibit similar behavior for the four alcohol molecules. In each case, a shift of the $\cos\theta_2$ values is observed from -0.9 to between -0.5 and -0.4 when increasing the coverage from System 1 to System 3, which indicates that the CO vector, initially pointing toward the ice surface when the adsorbed molecules are nearly isolated ($\theta_2 \sim 155°$), tend to orient more parallel to the ice surface at higher coverages. This reorientation of the CO vector is accompanied by a concomitant change in the orientation of the OH vector, as indicated by the split of the peak observed in $P(\cos\theta_3)$ upon increasing coverage. In fact, all these features can be attributed to the various possible orientations corresponding to the formation of proton donor and proton acceptor hydrogens bonds with the surface water molecules and, as the coverage increases, also with the neighboring alcohol molecules, as already simulated for methanol on ice (see Figure 10 of Ref.[24] for the illustration of the corresponding orientations).

To conclude this section, it appears from these analyses that the four alcohol molecules considered here exhibit similar orentational behavior at the ice surface, although the length of their aliphatic chain seems to impact on the orientation of the molecular axis, however, without changing the main features concerning their polar head.

IV. COMPARISON WITH EXPERIMENTS

Experimental measurements of the adsorption isotherm on ice are available at 228 K for the four alcohol molecules considered here.[47] The measured values of the surface concentrations Γ as a function of the pressure have thus been recorded from the original publication using WebPlotDigitizer[59] and are reported on Fig. 7 together with the corresponding simulated data at the same temperature (green curves), for comparison.

Overall, the simulated and measured isotherms exhibit very similar shape for ethanol and n-propanol although, for these molecules, the experiments have been limited to the low pressure range. The comparison appears to be a little bit less satisfactory for n-butanol and n-pentanol, especially at higher pressures, although it should be noticed that for these molecules the scattering of the experimental data in the range of $[10^{-3} - 10^{-2}]$ Pa does not allow any definite conclusion to be drawn. Additional experimental data related to multilayer adsorption have also been obtained for n-pentanol, above 10^{-2} Pa.[47] However, at these pressure values, simulated data do not show any evidence either for condensation or multilayer adsorption, a feature that may be related to the likely overestimation of the P_0 value for n-pentanol by the interaction potential model used in the present GCMC calculations, as discussed in a previous sub-section.

In fact, The results given in Fig. 7 at 228 K may evidence a small temperature shift between the simulated and measured isotherms, as already obtained when modeling the adsorption of methanol on ice.[24] Thus, to investigate this feature, we have performed additional simulations at various temperatures, above 228 K. The corresponding results are given in Fig. 7 for the four alcohols molecules considered here (red curves). First, it clearly appears from the comparison between experimental and simulated isotherms for ethanol (Fig. 7a) that the GCMC data obtained at 233 K exhibit an excellent agreement with the experimental results in the whole pressure range for which such data are available (see the inset in Fig. 7a). However, because the experimental ice surface could be not as perfect as in the simulations, we cannot exclude that such an agreement could be, at least partly, fortuitous. Nevertheless, taking into account the simulated results at 228 and 233 K, we can conclude that, in the case of ethanol, the AUA4 potential model used is accurate enough not to lead to a shift larger than 5 K with respect to the experimental results.

A similar conclusion can be drawn for n-propanol (Fig. 7b), considering that the experimental isotherm, measured at 228 K, is perfectly fitted by the simulated isotherm at 233 K, at least in the low pressure range (see the inset in Fig. 7b). At higher pressures, the agreement is a little bit less satisfactory, although the rather large scattering of the experimental data should again be pointed out. Thus, as for ethanol, here we can infer that the accuracy of the AUA4 potential model could lead to a shift that is likely not larger than 5 K when considering the adsorption isotherm of n-propanol molecules on ice.

For n-butanol and n-pentanol, the situation appears to be a little bit more confused. Indeed, while the best agreement with the experimental isotherms recorded at 228 K is obtained for the simulated ones at 233 K in the low pressure range (Fig. 7c and Fig. 7d), these simulated isotherms clearly overestimate the number of adsorbed molecules at larger pressure values. Thus, simulations up to 238 K (for n-butanol, see Fig. 7c) or even to 245 K (for n-pentanol, see Fig. 7d) are required to get a better agreement with the experiments in this pressure range, although, as already mentioned above, the pertinence of the measurements could also be questioned in the high pressure range for these molecules due to the large scattering of the recorded data (especially for n-pentanol). Hence, from the present comparison with experimental data available at 228 K, we can conclude that, for the larger alcohol molecules, the accuracy of the AUA4 potential model could lead to a shift not larger than 5 K at low coverages, and of about 10 K at pressures corresponding to the saturation of one monolayer of adsorbed molecules on ice.

Thus, it is tempting to infer from these comparisons that the longer the carbon chain is, the less accurate

is the AUA4 potential model, at least when used for studying adsorption on ice. However, it is important to emphasize that this conclusion questions the representation of the aliphatic chain rather than that of the polar head of these alcohol molecules. Indeed, in the low pressure range (i.e., at low coverages), where the adsorption phenomenon is mainly driven by the interaction of the polar head of the alcohol molecules with ice, the simulated isotherms of all the four molecules considered show excellent agreement with the experimental data, within an accuracy range of at most 5 K. By contrast, at larger pressures (i.e., higher coverages), when the interaction between the aliphatic chains of the neighboring molecules starts to play a non-negligible role (see Fig. 4), a better agreement with experiments is obtained for the small than for the large alcohol molecules. It should be mentioned that the better performance of ethanol and n-propanol at the highest fugacity values considered here could, at least in part, also come from a better sampling of the configurational space, in particular due to easier insertion of these small molecules into dense media, compared to the larger n-butanol and n-pentanol molecules.

Finally, to complete the present study, experimental data obtained at temperatures other than 228 K for ethanol, n-butanol and n-pentanol can also be considered. Thus, in Fig. 8, all the available measured isotherms (except that at 228 K) are compared to the simulated curves, including additional simulation results obtained at 213 and 221 K. Again, an overall very good agreement is found for ethanol, irrespective of the temperature, when taking into account a likely shift of no more than 5 K between simulations and experiments. The situation is also quite satisfactory when considering n-butanol, especially in the low pressure range. Indeed, for this species, the experimental isotherm measured at 213 K falls between the simulated curves at 213 and 221 K. Similarly, the experimental isotherm obtained at 221 K falls between the isotherms simulated at 221 and 228 K, while the one measured at 233 K falls between the simulated ones at 233 and 238 K. Thus, from these comparison, the accuracy of the AUA4 potential model for n-butanol could be estimated of being below $5-7$ K in the pressure range corresponding to low surface coverages, i.e., when the interaction of the alcoholic group with ice plays the main role in the adsorption process. No such clear conclusion can be drawn for the larger n-pentanol molecule considering, on one hand, the large scattering of the measured data and, on the other hand, the failure of the present simulations at correctly representing the experimental isotherms at 221 and 228 K in the pressure range for which multilayer adsorption has been evidenced. However, in the low pressure range, below the saturation of the monolayer, the simulated isotherms for n-pentanol exhibit a similar shape than the experimental ones, when taking into account a temperature shift that does not exceed $8-10$ K.

V. CONCLUSIONS

Here, the adsorption of four linear alcohol molecules on crystalline ice has been characterized by using GCMC simulations, performed with the transferable AUA4 interaction potential model. Various temperatures have been considered in the simulations, for comparison with the available experimental data. The results of the simulations turned out to be in very good agreement with the major features provided by the experimental measurements, especially at low coverage, when the lateral interactions within the adsorbed layer do not play any significant role and the adsorption process is mainly driven by the interaction with the ice substrate, provided that a small temperature shift between simulations and experiments is taken into account. In this situation, the polar head of the adsorbed molecules tend to optimize its hydrogen bonding with the surrounding water molecules of the ice substrate, whereas the aliphatic chains lie more or less parallel to the ice surface. Upon coverage increase up to saturation, the alcohol-alcohol interactions become even more important than the alcohol-water ones. Correspondingly, the preferred orientation of the adsorbed molecules changes from parallel to perpendicular to the ice surface, their aliphatic methyl group pointing up to the gas phase. Nevertheless, the polar head of the alcohol molecules always remains in close contact with the ice substrate, irrespective of the pressure, up to the 3D condensation of the adsorbate. In the low pressure range, *i.e.*, below saturation of one adsorbed layer on the surface, simulated and measured adsorption isotherms exhibit a noticeable very good agreement, when taking into account a possible temperature shift of no more than a few K between experimental and simulated results. Meanwhile, the comparison between experimental and simulated isotherms is a little bit less satisfactory at higher pressures and for the largest n-butanol and n-pentanol molecules. This feature points out that a possible weakness of the AUA4 interaction potential is to accurately describe the long aliphatic chains. This could be related to an underestimation of the lateral interactions between the large alcohol molecules, as reflected in the too large values of the simulated pressures of the saturated vapor with respect to the corresponding experimental values for n-butanol and n-pentanol.

Nevertheless, the observed overall agreement of the simulated and experimental isotherms confirms the validity of the numerical model used here. Moreover, the main conclusions of the present study, concerning the adsorption energy, the balance between U_{ads-w} and $U_{ads-ads}$ when the surface coverage increases, the orientations of the adsorbed molecules as well as the ability of ethanol molecules to form multiple adsorbed layers before condensation occurs, nicely agree with the very recent results obtained with quantum calculations based on the fragment molecular orbital method.[60] Thus, the present GCMC approach can be safely used to analyze in detail the properties of adsorption layer on ice and use-

fully complement the information that are issued from the measurements. Finally, it is worth noting that the accuracy of the AUA4 model, especially in the low pressure range, as tested in the present study in tropospheric conditions, opens the way for its use in modeling studies also relevant to an astrophysical context where molecular concentrations are usually low, and for which experimental measurements are, at present, missing.

ACKNOWLEDGMENTS

This project has been financially supported by the Région Bourgogne Franche-Comté which is gratefully acknowledged (project number 2020Y-11942). PJ acknowledges financial support from the NKFIH Foundation, Hungary (project number 134596). Computations have been performed on the supercomputer facilities of the Mésocentre de calcul de Franche-Comté.

DATA AVAILABILITY STATEMENT

The data that support the findings of this study are available from the corresponding author upon reasonable request.

[1] B. A. McGuire, Astrophys. J. Supp. Ser. **239**, 17 (2018).
[2] A. C. A. Boogert, P. A. Gerakines, and D. C. B. Whitte, Ann. Rev. Astron. Astrophys. **53**, 541–581 (2015).
[3] T. Encrenaz, *Searching for Water in the Universe* (Springer-Verlag New York, 2007).
[4] P. de Marcellus, C. Meinert, I. Myrgorodska, L. Nahon, T. Buhse, L. L. S. d'Hendecourt, and U. J. Meierhenrich, PNAS **112**, 965–970 (2015).
[5] A. Fresneau, N. A. Mrad, L. L. S. d'Hendecourt, F. Duvernay, L. Flandinet, F.-R. Orthous-Daunay, V. Vuitton, R. Thissen, T. Chiavassa, and G. Danger, Astrophys. J. **837**, 168 (2017).
[6] E. Herbst, Phys. Chem. Chem. Phys. **16**, 3344–3359 (2014).
[7] H. M. Cuppen, C. Walsh, T. Lamberts, D. Semenov, R. T. Garrod, E. M. Penteado, and S. Ioppolo, Space Sci Rev. **212**, 1–58 (2017).
[8] M. S. Gudipati and J. Castillo-Rogez, eds., (Springer, New York, NY, USA, 2013).
[9] H. Tanaka, T. Yagasaki, and M. Matsumoto, Planet. Sci. J. **1**, 80 (2020).
[10] M. Ammann, P. Ariya, T. Bartels-Rausch, F. Domine, D. J. Donaldson, M. I. Guzman, D. Heger, T. F. Kahan, P. Klán, S. Masclin, C. Toubin, and D. Voisin, Atmos. Chem. Phys. **12**, 9653–9678 (2012).
[11] O. Mousis, E. Chassefière, N. Holm, A. Bouquet, J. H. Waite, W. D. Geppert, S. Picaud, Y. Aikawa, M. Ali-Dib, P. Rousselot, and L. Ziurys, Astrobiol. **15**, 308–326 (2015).
[12] A. Bouquet, C. Glein, and J. H. Waite, Astrophys. J. **873**, 28 (2019).
[13] S. Solomon, Rev. Geophys. **37**, 275–316 (1999).
[14] P. J. Crutzen and M. G. Lawrence, J. Atmos. Chem. **37**, 81–112 (2000).
[15] J. P. D. Abbatt, Chem. Rev. **103**, 4783–4800 (2003).
[16] T. Huthwelker, M. Ammann, and T. Peter, Chem Rev. **106**, 1375–1444 (2006).
[17] C. E. Kolb, R. A. Cox, J. P. D. Abbatt, M. Ammann, E. J. Davis, D. J. Donaldson, B. C. Garrett, C. George, P. T. Griffiths, D. R. Hanson, M. Kulmala, G. McFiggans, U. Pöschl, I. Riipinen, M. J. Rossi, Y. Rudich, P. E. Wagner, P. M. Winkler, D. R. Worsnop, and C. D. O'Dowd, Atmos. Chem. Phys. **10**, 10561–10605 (2010).
[18] T. Bartels-Rausch, H.-W. Jacobi, T. F. Kahan, J. L. Thomas, E. S. Thomson, J. P. D. Abbatt, M. Ammann, J. R. Blackford, H. Bluhm, C. Boxe, and *et al.*, Atmos. Chem. Phys. **14**, 1587–1633 (2014).
[19] S. Ferrero, L. Zamirri, C. Ceccarelli, A. Witzel, A. Rimola, and P. Ugliengo, Astrophys. J. **904**, 11 (2021).
[20] C. Czech, S. M. Hammer, B. Bonn, and M. U. Schmidt, Atmos. Environ. **45**, 687–693 (2011).
[21] S. Picaud and P. Jedlovszky, Mol. Sim. **45**, 403–416 (2019).
[22] D. J. Adams, Mol. Phys. **29**, 307–311 (1975).
[23] M. P. Allen and D. J. Tildesley, *Computer simulation of liquids* (Oxford university press, 2017).
[24] P. Jedlovszky, L. Pártay, P. N. M. Hoang, S. Picaud, P. von Hessberg, and J. N. Crowley, J. Am. Chem. Soc. **128**, 15300–15309 (2006).
[25] G. Hantal, P. Jedlovszky, P. N. M. Hoang, and S. Picaud, J. Phys. Chem. C **111**, 14170–14178 (2007).
[26] G. Hantal, P. Jedlovszky, P. N. M. Hoang, and S. Picaud, Phys. Chem. Chem. Phys. **10**, 6369–6380 (2008).
[27] P. Jedlovszky, G. Hantal, K. Neuróhr, S. Picaud, P. N. M. Hoang, P. V. Hessberg, and J. N. Crowley, J. Phys. Chem. C **112**, 8976–8987 (2008).
[28] M. Petitjean, G. Hantal, C. Chauvin, P. Mirabel, S. L. Calvé, P. N. M. Hoang, S. Picaud, and P. Jedlovszky, Langmuir **26**, 9596–9606 (2010).
[29] M. Darvas, J. Lasne, C. Laffon, P. Parent, S. Picaud, and P. Jedlovszky, Langmuir **28**, 4198–4207 (2012).
[30] Z. Meszar, G. Hantal, S. Picaud, and P. Jedlovszky, J. Phys. Chem. C **117**, 6719–6729 (2013).
[31] M. Szori and P. Jedlovszky, J. Phys. Chem. C **118**, 3599–3609 (2014).

[32]S. Picaud and P. Jedlovszky, Chem. Phys. Lett. **600**, 73–78 (2014).
[33]I. Sumi, S. Picaud, and P. Jedlovszky, J. Phys. Chem. C **119**, 17243–17252 (2015).
[34]V. Szentirmai, M. Szöri, S. Picaud, and P. Jedlovszky, J. Phys. Chem. C **120**, 23480–23489 (2016).
[35]I. Sumi, B. Fábián, S. Picaud, and P. Jedlovszky, J. Phys. Chem. C **120**, 17386–17399 (2016).
[36]I. Sumi, S. Picaud, and P. Jedlovszky, J. Phys. Chem. C **121**, 7782–7793 (2017).
[37]Z. Fu, N. He, P. Zhou, J. Liu, H.-B. Xie, Q. Yu, F. Ma, Z. Fu, Z. Wang, and J. Chen, J. Phys. Chem. C **121**, 15746–15755 (2017).
[38]R. A. Horváth, G. Hantal, S. Picaud, M. Szöri, and P. Jedlovszky, J. Phys. Chem. A **122**, 3398–3412 (2018).
[39]Z. Fu, N. He, P. Zhou, H.-B. Xie, Z. Fu, C. Liu, and J. Chen, J. Mol. Liq. **290**, 111221 (2019).
[40]B. Kiss, S. Picaud, M. Szöri, and P. Jedlovszky, J. Phys. Chem. A **123**, 2935–2948 (2019).
[41]B. Kiss, M. Szöri, and P. Jedlovszky, J. Phys. Chem. C **124**, 16402–16414 (2020).
[42]P. Jedlovszky, R. A. Horváth, and M. Szöri, J. Phys. Chem. C **124**, 10615–10626 (2020).
[43]J. Joliat, A. Patt, J.-M. Simon, and S. Picaud, Mol. Sim. **48**, 19–30 (2022).
[44]A. Mellouki, T. Wallington, and J. Chen, Chem. Rev. **115**, 3984–4014 (2015).
[45]B. A. Magee and J. H. Waite, in *Lunar and Planetary Science Conference*, 1964 (2017) p. 2974.
[46]N. Ferrando, V. Lachet, J.-M. Teuler, and A. Boutin, J. Phys. Chem. B **113**, 5985–5995 (2009).
[47]O. Sokolov and J. P. D. Abbatt, J. Phys. Chem. A **106**, 775–782 (2002).
[48]V. Buch, P. Sandler, and J. Sadlej, J. Phys. Chem. B **102**, 8641–8653 (1998).
[49]J. L. F. Abascal, E. Sanz, R. G. Fernández, and C. Vega, J. Chem. Phys. **122**, 234511 (2005).
[50]M. M. Conde, M. Rovere, and P. Gallo, J. Chem. Phys. **147**, 244506 (2017).
[51]D. Frenkel and B. Smit, *Understanding Molecular Simulation: from Algorithms to Applications*, Vol. 1 (Elsevier, 2001).
[52]A. D. Fortes, Acta Crystallogr. B **74**, 196–216 (2018).
[53]P. Ungerer, B. Tavitian, and A. Boutin, *Applications of Molecular Simulation in the Oil and Gas Industry: Monte Carlo Methods* (Editions Technip, 2005).
[54]A. Patt and S. Picaud, ACS Earth and Space Chem. **5**, 1782–1791 (2021).
[55]B. Widom, J. Chem. Phys. **39**, 2808–2812 (1963).
[56]P. J. Linstrom and E. W. G. Mallard, *NIST Chemistry WebBook, NIST Standard Reference Database Number 69* (National Institute of Standards and Technology, Gaithersburg MD, 20899).
[57]C. L. Yaws, *The Yaws Handbook of Vapor Pressure: Antoine Coefficients.* (Gulf Professional Publishing, Oxford, 2015).
[58]P. Jedlovszky, A. Vincze, and G. Horvai, J. Chem. Phys. **117**, 2271–2280 (2002).
[59]A. Rohatgi, "Webplotdigitizer: Version 4.5," (2021), `https://automeris.io/WebPlotDigitizer`.
[60]T. Nakamura, T. Yokaichiya, and D. G. Fedorov, J. Phys. Chem. A **126**, 957–969 (2022).

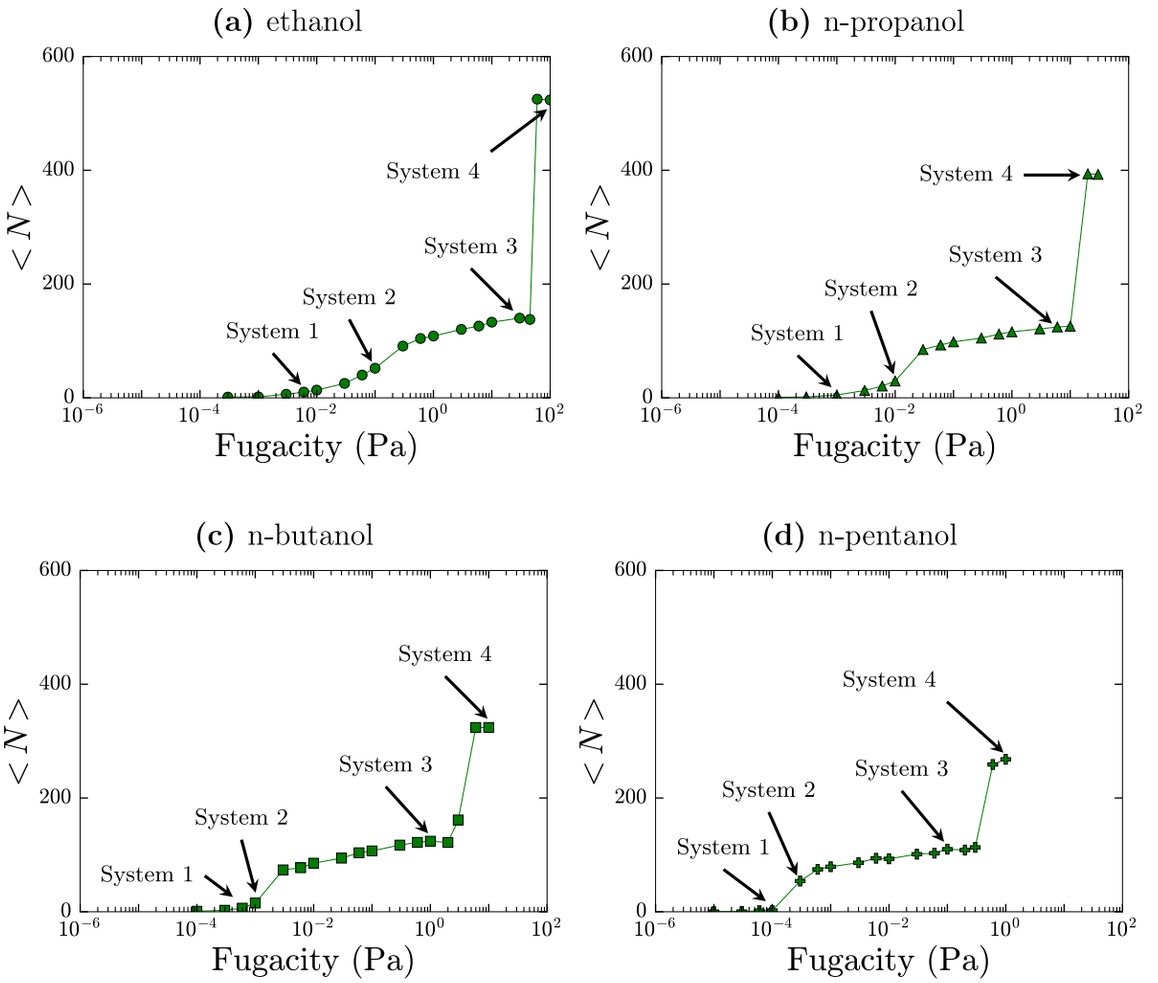

FIG. 1. Average number of (a) ethanol, (b) n-propanol, (c) n-butanol, and (d) n-pentanol molecules in the basic simulation box as a function of the fugacity (note that the errors bars are smaller than the symbols), as calculated from the present GCMC simulations at 228 K. The arrows indicate the systems used in the detailed analyses. Lines are only guide to the eye.

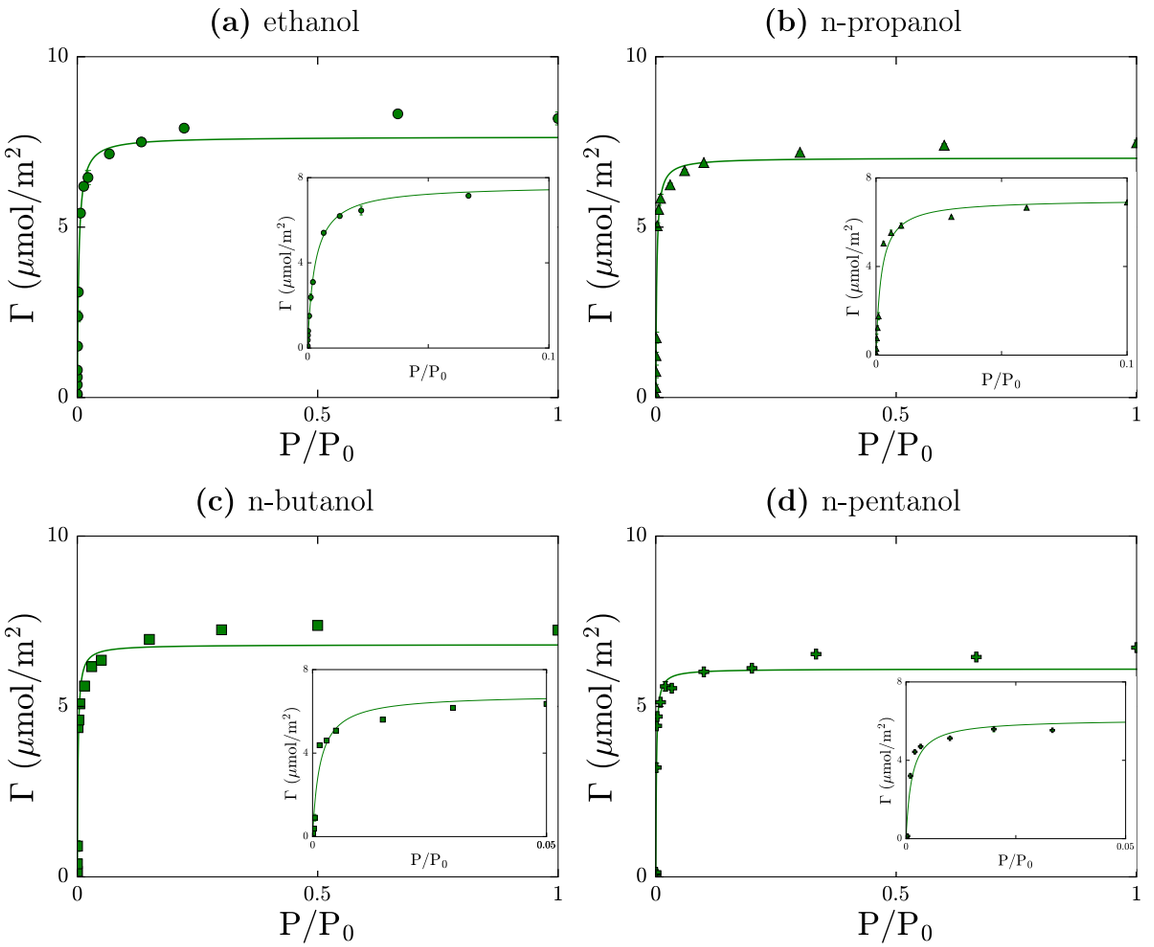

FIG. 2. Langmuir fit of the simulated data (best t) for the adsorption isotherms of (a) ethanol, (b) n-propanol, (c) n-butanol, and (d) n-pentanol adsorbed on ice at 228 K. Inserts show the range of relative pressure in which the best Langmuir t can be achieved from the simulation data.

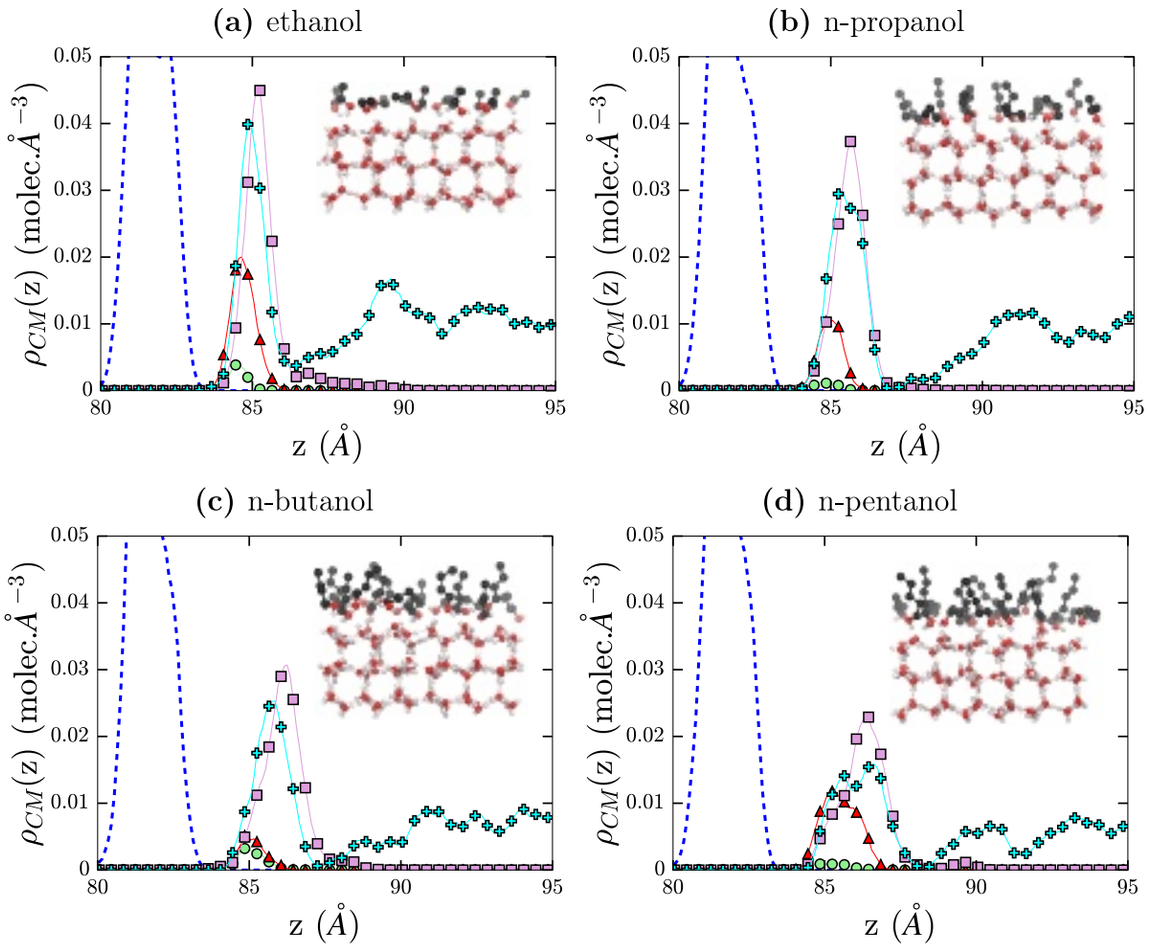

FIG. 3. Number density prole for (a) ethanol, (b) n-propanol, (c) n-butanol, and (d) n-pentanol centers of mass, in Systems 1 (green circles), 2 (red triangles), 3 (pink squares) and 4 (blue crosses), as obtained from the simulations at 228 K. For reference, the outer tail of the number density prole of the water centers of mass in System 1 is also given (dashed blue line). In addition, snapshots issued from the simulations of System 3 are given, to illustrate the adsorption geometry when the alcohol molecules form a nearly saturated monolayer at the ice surface. In these snapshots, red, white, and black (gray) circles represent oxygen, hydrogen and carbon (bottom carbon) atoms, respectively. Note that hydrogen atoms of the aliphatic chains are not explicitly included in the united atom AUA4 potential model and, thus, they are not shown.

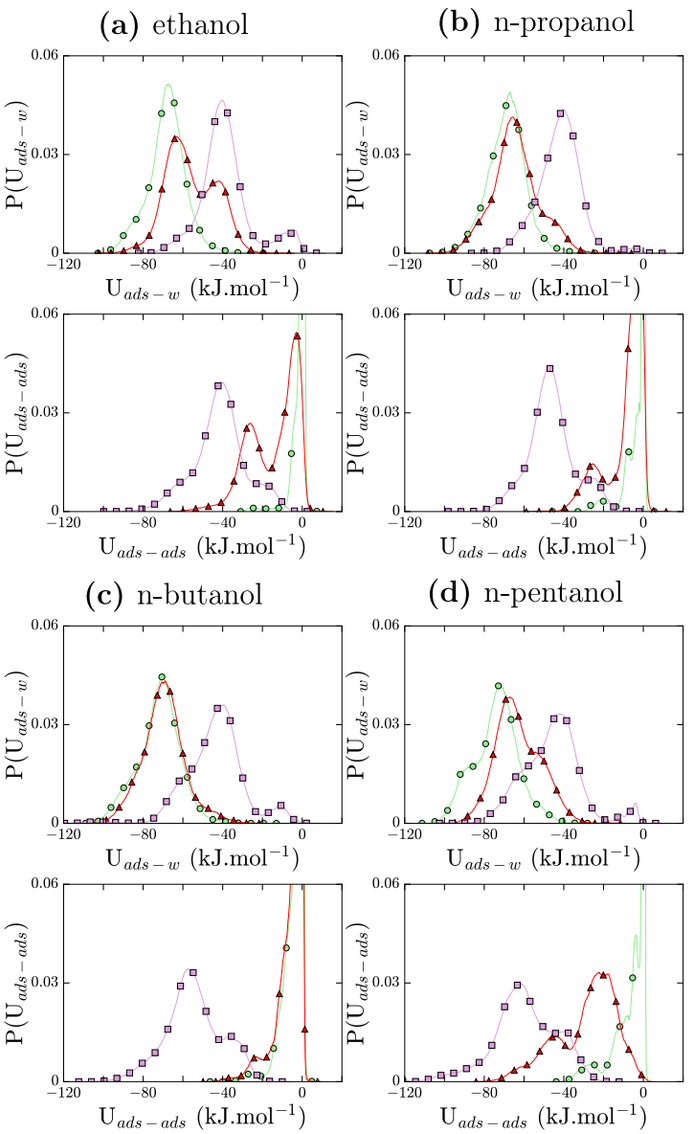

FIG. 4. Distribution of the interaction energy of an adsorbed (a) ethanol, (b) n-propanol, (c) n-butanol and (d) n-pentanol molecule with the ice phase $P(U_{ads-w})$ and with the other adsorbed molecules $P(U_{ads-ads})$ for Systems 1 (green circles), 2 (red triangles) and 3 (pink squares).

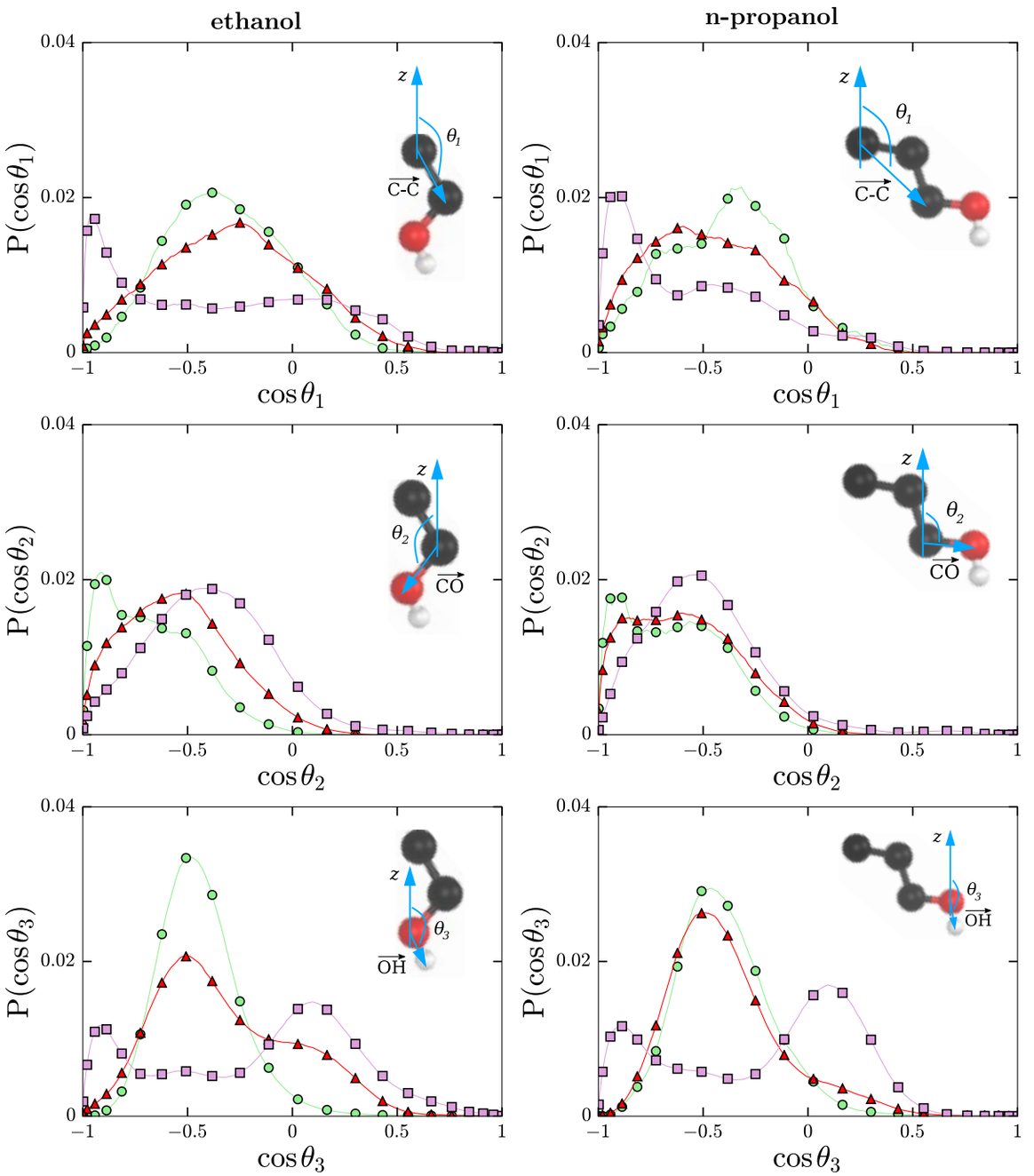

FIG. 5. Distribution of the molecular orientations for ethanol (left) and n-propanol (right) molecules adsorbed on ice, for Systems 1 (green circles), 2 (red triangles) and 3 (pink squares). Top row: θ_1 is the angle formed between the C-C vector and surface normal vector (z); middle row: θ_2 is the angle formed between the CO vector and z; bottom row, θ_3 is the angle formed between the OH vector and z. Inserts show the definition of the various angles considered.

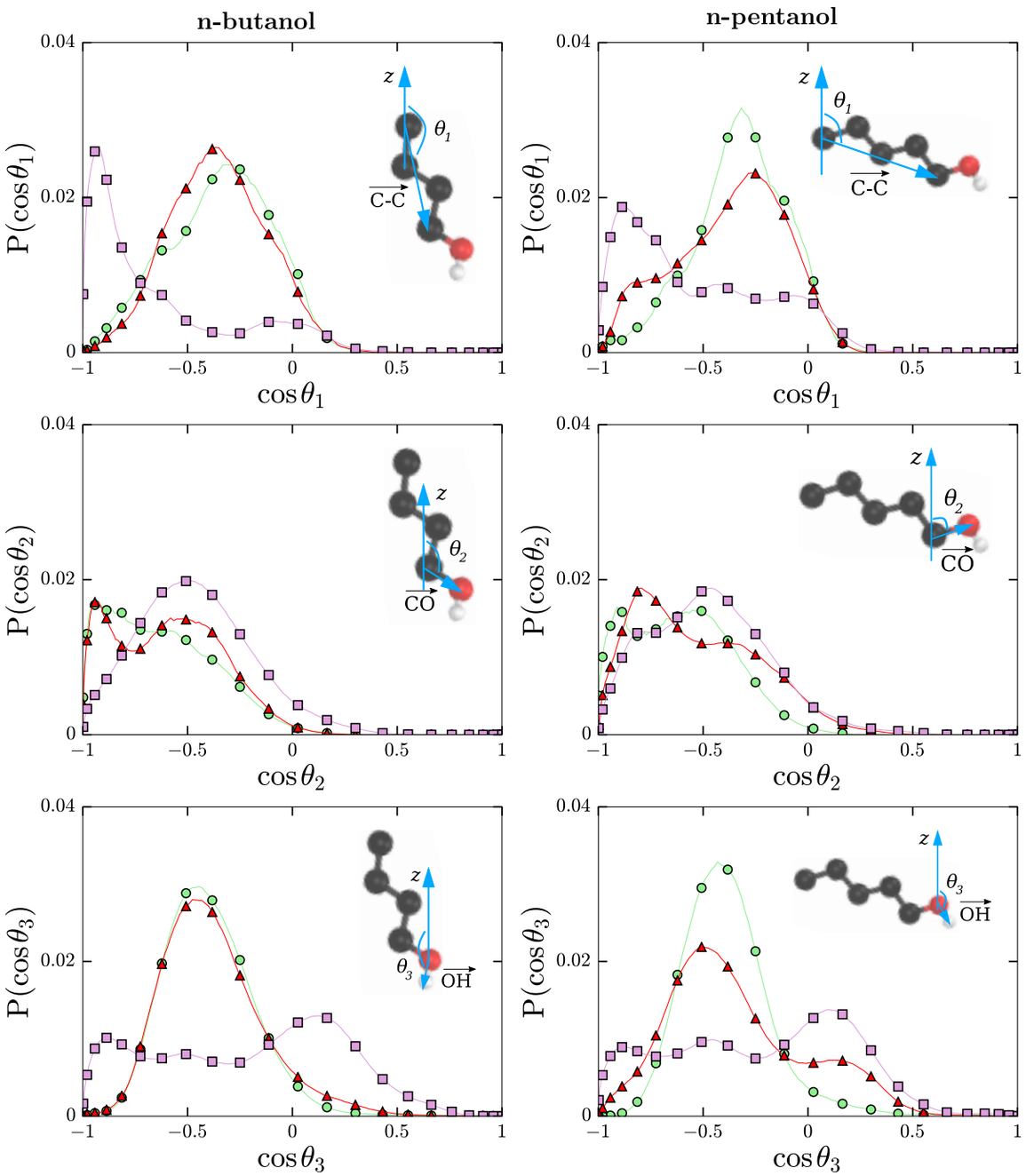

FIG. 6. Distribution of the molecular orientations for n-butanol (left) and n-pentanol (right) molecules adsorbed on ice, for Systems 1 (green circles), 2 (red triangles) and 3 (pink squares). Top row: θ_1 is the angle formed between the the C-C vector and surface normal vector (z); middle row: θ_2 is the angle formed between the CO vector and z; bottom row, θ_3 is the angle formed between the OH vector and z. Inserts show the definition of the various angles considered.

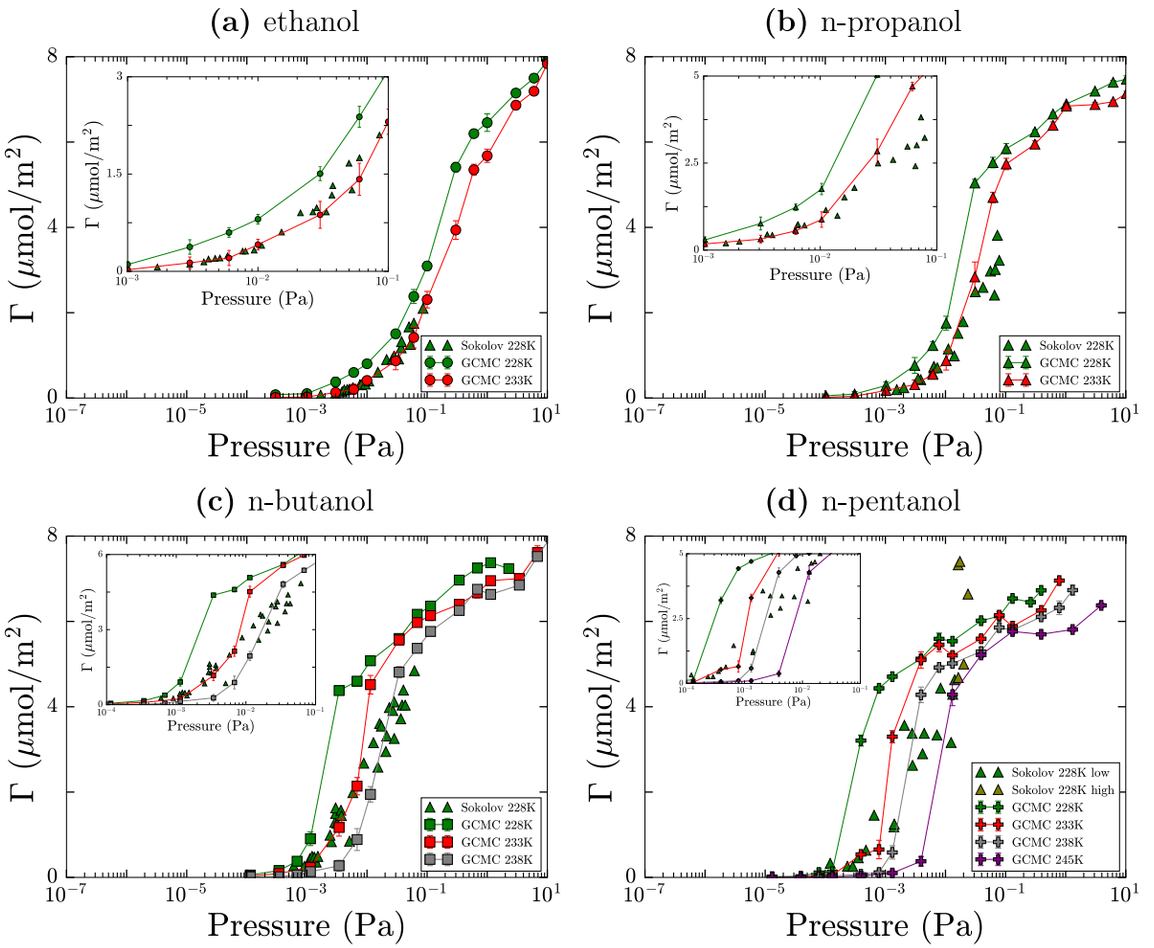

FIG. 7. Comparison between the experimental data recorded at 228 K and the adsorption isotherms of (a) ethanol, (b) n-propanol, (c) n-butanol, and (d) n-pentanol molecules on ice simulated at various temperatures. Lines are only guide to the eye.

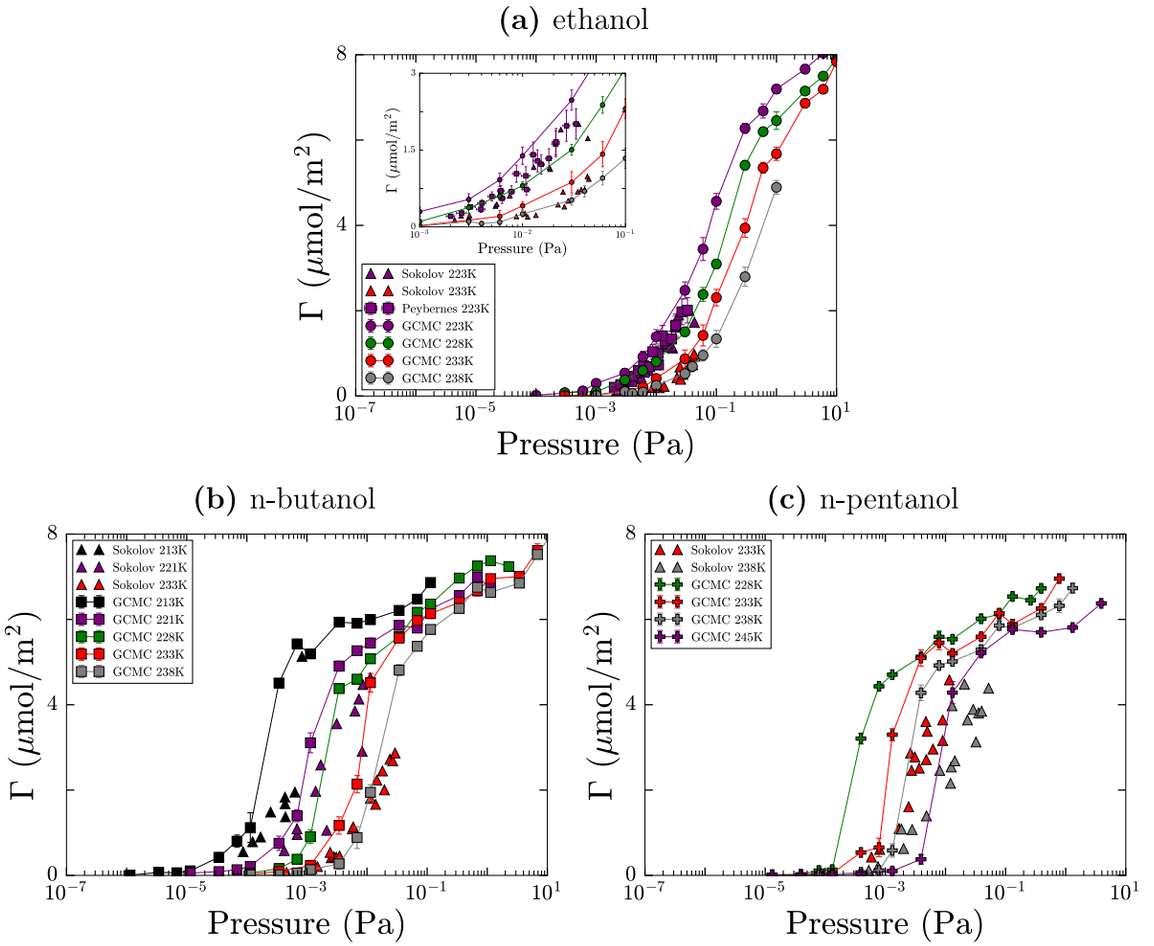

FIG. 8. Comparison between the experimental data recorded at various temperatures for (a) ethanol, (b) n-butanol, and (c) n-pentanol and some of the corresponding simulated adsorption isotherms. Lines are only guide to the eye.

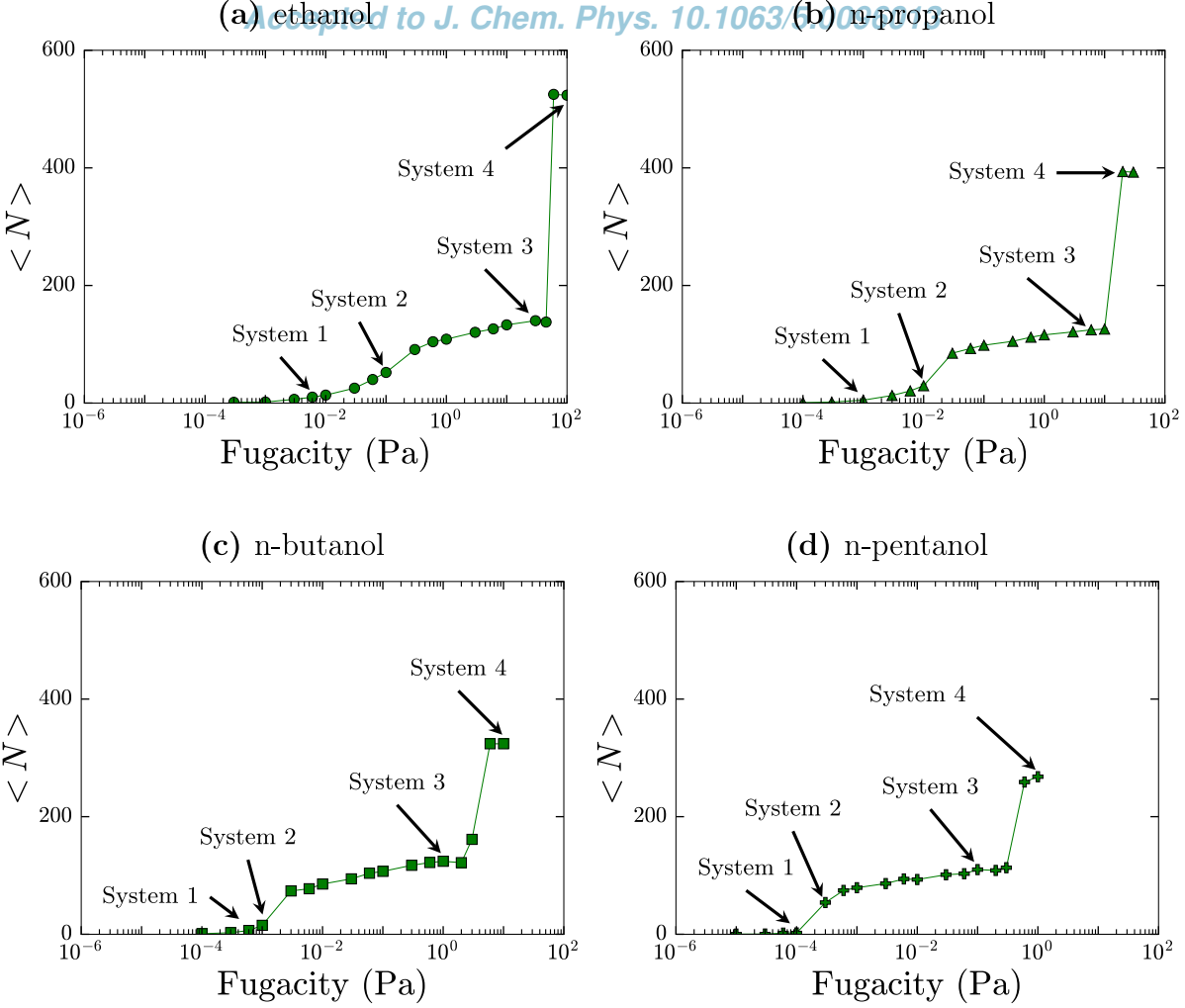

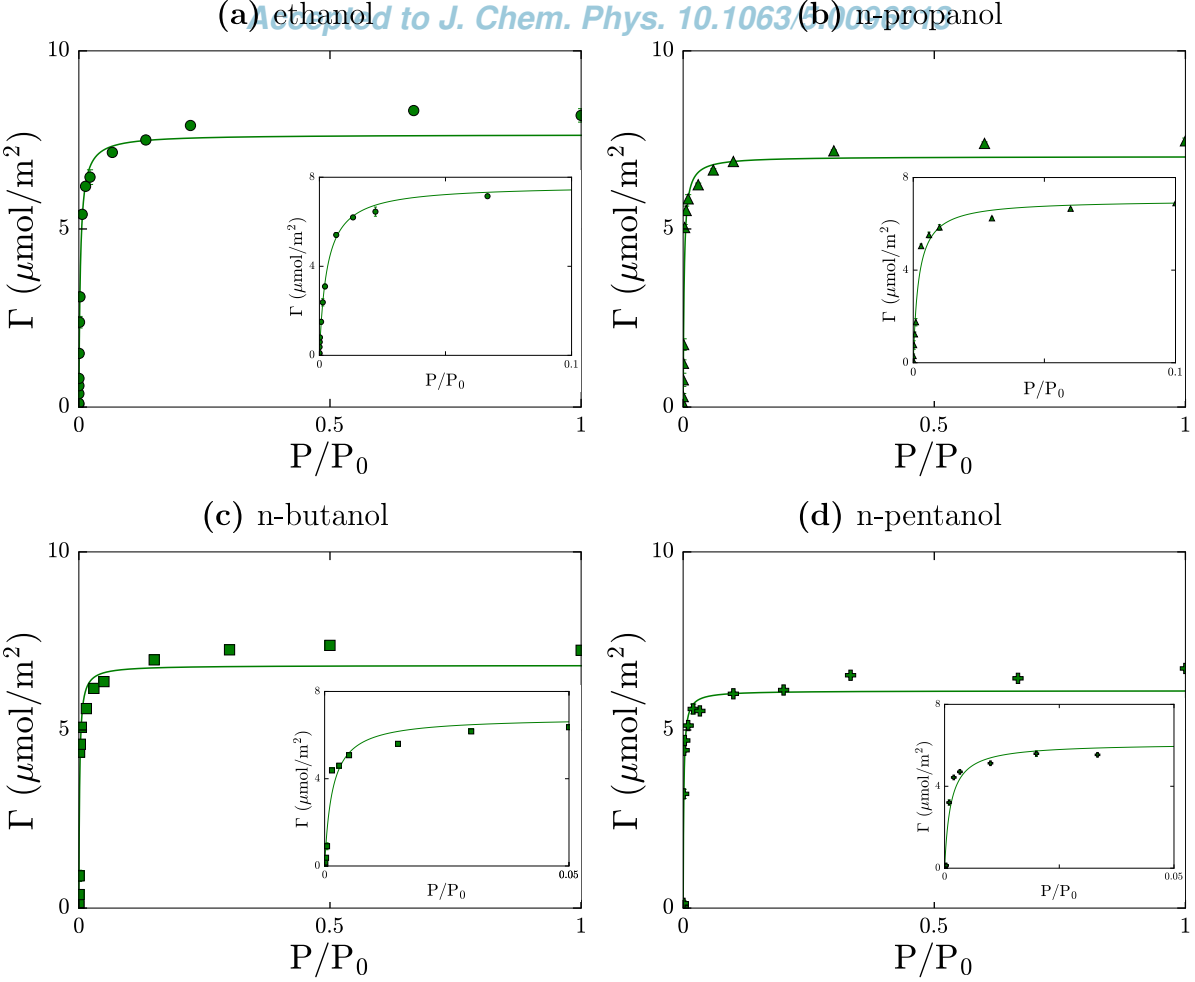

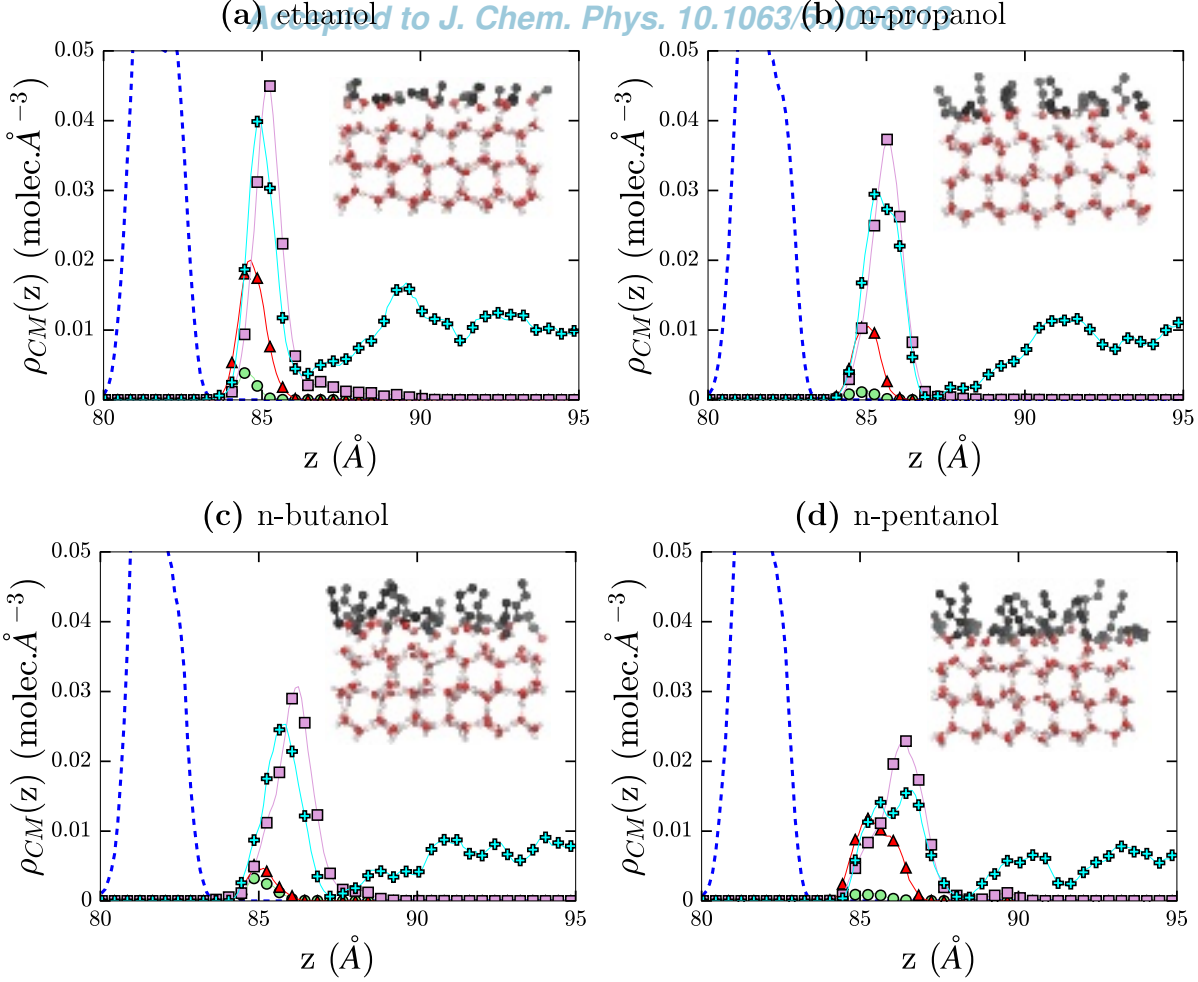

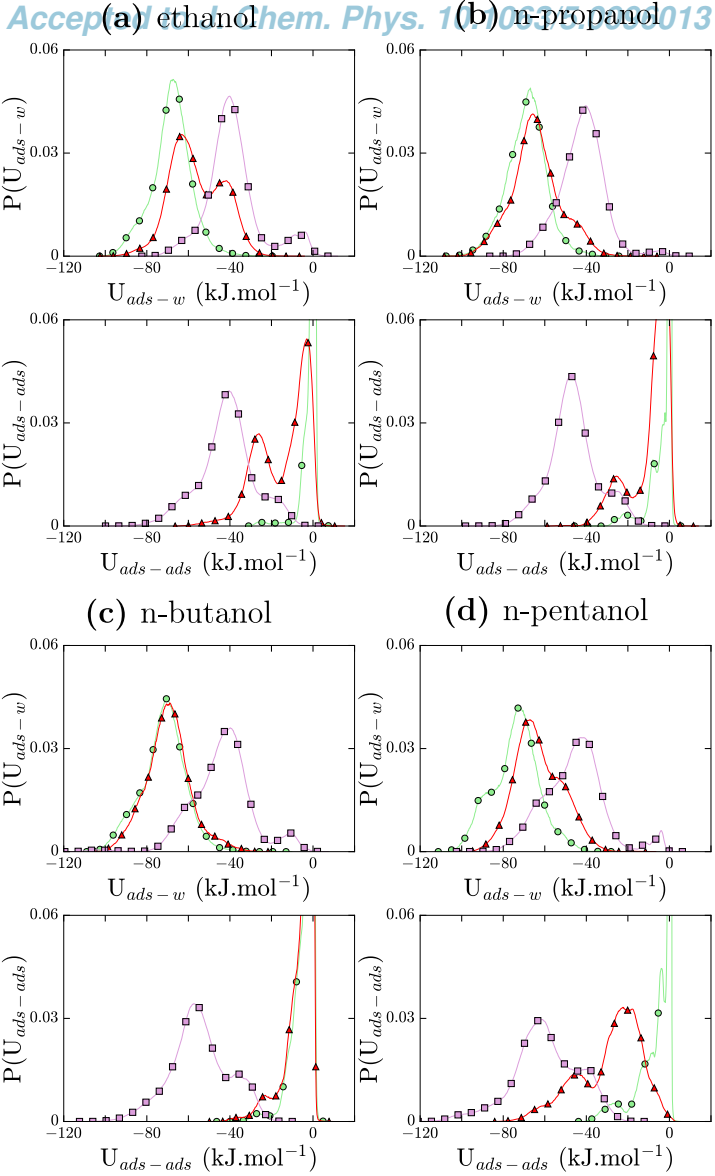

ethanol n-propanol